Since January 2020 Elsevier has created a COVID-19 resource centre with free information in English and Mandarin on the novel coronavirus COVID-19. The COVID-19 resource centre is hosted on Elsevier Connect, the company's public news and information website.

Journal of the Indian Chemical Society 99 (2022) 100697

Contents lists available at ScienceDirect

Journal of the Indian Chemical Society

journal homepage: www.journals.elsevier.com/journal-of-the-indian-chemical-society

Evaluation of flavonoids as potential inhibitors of the SARS-CoV-2 main protease and spike RBD: Molecular docking, ADMET evaluation and molecular dynamics simulations

Hanine Hadni *, Asmae Fitri, Adil Touimi Benjelloun, Mohammed Benzakour, Mohammed Mcharfi

LIMAS, Faculty of Sciences Dhar El Mahraz, Sidi Mohamed Ben Abdellah University, Fez, Morocco

ARTICLE INFO

Keywords:
SARS-CoV-2
Molecular docking
Flavonoid family
ADMET properties
Druglikeness
Molecular dynamics simulation
MM-GBSA study

ABSTRACT

The 3CLpro main protease and the RDB spike (*s*) protein of SARS-CoV-2 are critical targets in the treatment of coronavirus 19 disease (COVID-19), as they are responsible for the COVID-19 replication and infection. With this in mind, Molecular docking of 26 natural compounds belonging to the flavonoid family with the 3CLpro and RBD sites of SARS-CoV-2 has been performed. The docking results revealed that the ligands Silibinin, Tomentin A, Tomentin B, 4′-O-methyldiplacone, Hesperidin Amentoflavone and Bilobetin act as a potential inhibitor of SARS-CoV-2 3CLpro, and that the ligands Herbacetin, Morin, Silibinin, Tomentin E, Amentoflavone, Bilobetin, Baicalein and Quercetin can be potential inhibitors of SARS-CoV-2 RBD. It has been noticed that three ligands can inhibit both sites of SARS-CoV-2, indicating a great potential of these compounds to combat COVID-19. Moreover, molecular docking has been validated by a new validation method based on visual inspiration. Evaluation of ADMET pharmacokinetic properties and the drug likeness in silico revealed that six compounds could be effective drugs against COVID-19. Finally, the docking results were verified by molecular dynamics simulations and MM-GBSA calculation to confirm the stability of hydrogen bonding interactions with crucial residues, which are essential to overcome SARS-CoV-2. These results could direct researchers toward plant-derived compounds that could be further investigated as therapeutic targets against COVID-19 replication and infection.

1. Introduction

In December 2019, an unidentified pneumonia case was first reported in Wuhan city of China. A month later, this disease was identified as SARS-CoV-2, which was declared a COVID-19 pandemic a few days later by WHO [1,2]. This emerging infectious disease is caused by coronavirus strain provokes fever, coughing and breathing difficulties. Despite numerous vaccination efforts against COVID-19, the disease continues to spread worldwide, even in a country with a very high vaccination rate, causing 219 million infections and 4.55 million deaths worldwide up to the writing of this article [3–5].

Currently, several biological targets have been identified as potential therapeutic targets for SARS-CoV-2. Among them, the 3-chymotrypsin like protease (3CLpro) [6] and the receptor-binding domain (RBD) of the spike (S) protein [7] have been extensively investigated as therapeutic targets of the novel coronavirus. The main viral protease 3CLpro of the SRAS-CoV-2 plays a critical role in the life cycle of the novel coronavirus [8]. This enzyme is mainly involved in viral maturation and infection as it is required for coronavirus replication and transcription. Thus, inhibition of coronavirus main protease 3CLpro is considered a critical target for the development of antiviral drugs against COVID-19. On the other hand, Sars-CoV-2 uses the surface spike (S) glycoprotein to interact with human host cells via the receptor binding domain (RBD), which binds directly to angiotensin-converting enzyme 2 (ACE2) [9,10]. Therefore, the interaction between the viral protein and its receptor is a prerequisite for human infection with COVID-19 [11,12]. These two pharmacological targets are very effective in drug discovery to treat COVID-19. Indeed, 3CLpro and RBD of the spike protein (S) are the two major SARS-CoV-2 enzymes that play a crucial role in viral replication and propagation, making them promising targets for drug discovery against this virus.

Medicinal plants, especially those used in traditional medicine, have been an excellent and valuable source of natural molecules with diverse pharmacological properties for several decades [13,14]. Many of these

* Corresponding author.
E-mail address: hadni.hanine@yahoo.fr (H. Hadni).

https://doi.org/10.1016/j.jics.2022.100697
Received 3 June 2022; Received in revised form 6 August 2022; Accepted 25 August 2022
Available online 31 August 2022

natural molecules have been widely used due to their therapeutic effects, especially their antibacterial and antiviral properties. Recently, many studies have reported that natural products can be used to fight against COVID-19. In addition, molecular modeling has helped the researcher to understand the interactions of these natural agents with the viral life cycle, such as entry into the cell, replication and transcription of the virus in the host cell, as well as targeting host-specific viral interactions. In fact, the development of bioinformatics tools and services can accelerate drug discovery processes by shortening timelines and anticipating their potential affinity to many drug targets [15–17].

In recent years, the use of molecular simulation methods in chemoinformatics (chemical molecules) and structural bioinformatics (proteins) has produced very impressive results in the drug discovery process [18,19]. In this study, we have performed a molecular docking study to explore the potential inhibitory activity of some commonly used medicinal plants. Thus, the main objective of this study is to identify drug candidates against COVID-19 that could inhibit the 3CLpro and RBD enzymes of SARS-CoV-2. Furthermore, in order to assess their drug-like ability, each selected compound was evaluated using standard computational pharmacokinetics parameters (ADMET) and drug-likeness prediction. Finally, 100 ns MD simulations were performed to estimate the stability of the ligand-receptor under normal physiological conditions.

2. Material and methods

2.1. Ligand preparation

Flavonoids are the largest family of phenolic compounds, more than 8000 flavonoid compounds have been identified in 2019. Moreover, they are recognized as dietary supplements that promote health and prevent disease [20]. Several studies show that flavonoids may have protective effects against various diseases as they exhibit various biological activities (Table 1). In this study, the canonical SMILES of the studied compounds were taken from pubchem (https://pubchem.ncbi.nlm.nih.gov/). These compounds are Herbacetin, Morin, Puerarin, Daidzein, Silibinin, Tomentin A, Tomentin B, Tomentin C, Tomentin D, Tomentin E, 3′-O-methyldiplacol, 4′-O-methyldiplacol, 3′-O-methyldiplacone, 4′-O-methyldiplacone, Diplacone, Hesperetin, Hesperidin, Nobiletin, Galangin, Myricetin, amentoflavone, Bilobetin, Naringenin, Baicalein, Quercetin and kaempferol (Table 1). The canonical SMILES were imported into ChemBioOffice software to obtain the 2D and 3D structures of the ligands. The 3D modeled structures were then subjected to geometry optimization and energy minimization using the MM2 Force Field until the RMS gradient value was less than 0.010 kcal/mol [21].

2.2. Protein preparation

The 3D crystal protein-structures of SARS-CoV-2 3CLpro (PDB ID: 6LU7) [41] and SARS-CoV-2 RBD of the spike (S) protein (PDB ID: 6M17) [42] were extracted from the RCSB PDB database (https://www.rcsb.org/). The 3D crystal structures of SARS-CoV-2 were prepared for molecular docking using Discovery Studio software to remove all ligands, non-protein parts and water molecules.

2.3. Docking molecular

Molecular docking simulation was carried out to analyze the protein-ligand interaction mechanism to obtain information about the binding affinity and ligand activity. In the present work, we performed the molecular docking analysis using AutoDock Tools and AutoDock 4.2 software [43], to analyze docked conformations and the interaction between the ligand and the protein. The 3D grid was generated by the AUTOGRID algorithm to evaluate the ligand-receptor interaction

Table 1
The bioactive compounds belong to the flavonoid family.

Compound	PubChem CID	Plant source	Activity
Herbacetin	5280544	*Linum usitatissimum* L	Anticancer, antibacterial, antidiabetic, anti-oxidant and anti-inflammatory activities [22]
Morin	5281670	*mulberry leaves, Osage orange and almond*	Anti-inflammatory, anticancer, anti-oxidant and antiviral activities [23,24]
Puerarin	5281807	*Kudzu*	Anticancer, antiparkinson's, anti-inflammatory, antidiabetic and antiviral activities [25]
Daidzein	5281708		Anti-oxidant, anti-inflammatory and anticancer activities [26]
Silibinin	31553	*milk thistle*	Anti-oxidant, anticancer, anti-inflammatory and antimicrobial activities [27]
Tomentin A	71659627	*Paulownia tomentosa*	Anti-inflammatory, anti-arthritic, antibacterial, anti-oxidant and antiviral activities [28,29]
Tomentin B	71659628		
Tomentin C	71659765		
Tomentin D	71659766		
Tomentin E	71659767		
3′-O-methyldiplacol	21607150		Anti-inflammatory, antileishmanial, antiparasitic, antiproliferative, anti-oxidant activities [30]
4′-O-methyldiplacol	24854124		
3′-O-methyldiplacone	14539951		
4′-O-methyldiplacone	24854122		
Diplacone	14539948		
Hesperetin	72281	*Citrus fruit*	Anti-oxidant, anti-inflammatory, anticancer and antimicrobial activities [31]
Hesperidin	10621		
Nobiletin	72344		Anti-inflammatory and anticancer activities [32]
Galangin	5281616	*Alpinia officinarum*	anti-inflammatory, antimicrobial, antiviral, *anti*-obesogenic and anti-oxidant activities [33]
amentoflavone	5281600	*Ginkgo biloba*	Anti-oxidant, anti-inflammatory, antisenescence, antitumor, antivirus and antifungal activities [34]
Bilobetin	5315459		Anti-oxidation, anticancer, antibacterial, antifungal, anti-inflammatory and antiviral activities [35]
Naringenin	932	*Lycopersicum esculentum*	Antidiabetic, anti-atherogenic, antidepressant, antitumor, anti-inflammatory activities [36]
Baicalein	5281605	*Scutellaria baicalensis and Scutellaria lateriflora*	Anti-inflammatory, anti-oxidant, antiviral and anticancer activities [37]
Myricetin	5281672	*onions, grapes, berries, cherries, broccoli and*	Anti-inflammatory, antitumor, antibacterial and antiviral activities [38]
Quercetin	5280343	*citrus fruits.*	Antihyperlipidemia, anti-oxidant, antiviral, anticancer, anti-inflammatory, antimicrobial activities [39]
kaempferol	5280863		Anti-oxidant, anti-inflammatory, anticancer, antidiabetic, and anti-aging activities [40]

energy. The defined coordinates of the SARS-CoV-2 3CLpro binding site region are located on the active site of Cys145 [44]. The grid maps were constructed with a value of 60 Å in all directions (X, Y, Z axes), with a default grid spacing of 0.375 Å, the Grid Coordinates for the main protease binding site determined as (x = −14.043, y = 17.445, z = 66.228). However, for the SARS-CoV-2 RBD binding site, the grid center is x = 171.662, y = 122.527 and z = 254.893, using the same grid box size. The established interaction analysis as well as the 2D and 3D visualizations were exploited using the BIOVIA Discovery Studio Visualizer 2020.

Molecular docking was validated by re-docking the crystallized ligand of the protein (PDB Id: 6lu7). Thus, the native ligand was separated from the receptor using BIOVIA Discovery Studio Visualizer 2020. Subsequently, we performed docking of the native ligand again with the same receptor. The lowest energy pose obtained from the docked ligand and the native ligand was superimposed, to obtain the root mean square distance (RMSD) value between these two superimposed ligands. Molecular docking is considered valid if the RMSD value obtained is less than 2 Å [45].

2.4. In silico pharmacokinetics ADMET and drug likeness prediction

The development of computer technology has allowed the development of new drug candidates, reducing the number of experimental studies and improving the success rate. For this reason, ADMET pharmacokinetic parameters and drug similarity have been determined for preliminary estimation in the drug discovery process. The in silico study provides a pathway to ADMET (Absorption, Distribution, Metabolism, Excretion and Toxicity) parameters [46], Its absorption of compounds in the human small intestine, distribution is the passage of compounds through the different tissues of the body, metabolism refers to the chemical biotransformation of a compound by the body, excretion is the elimination of a compound from the body and the level of toxicity of the compound. The prediction of the drug likeness to the selected compounds was estimated based on Lipinski, Ghose, Veber, Egan and Muegge rules.

2.5. Molecular dynamic simulation

Molecular dynamics (MD) simulations were performed using the Nanoscale Molecular Dynamics (NAMD) program [47]. The NAMD input files were generated on the CHARMM-GUI [48], using the CHARMM36 force field for the calculation of the system was solvated with the TIP3P water model [49] in a 10 Å cubic box around the protein and neutralised by the addition of the NaCl salt at the ionic concentration of 0.154 M using the Monte-Carlo method for ion positioning [50]. The energy was minimised for 10,000 steps using the steepest descent method. After minimization, the system was equilibrated at 310 K for 100 ns in a constant atom number, volume and temperature (NVT) ensemble. Then, the system was subjected to 100 ns of unrestricted MD simulations in a constant number of atoms, pressure, and temperature (NPT) ensemble with a reference temperature (310 K) and pressure (1 atm). The MD trajectory analyses were used to generate the root mean square deviation (RMSD), root mean square fluctuation (RMSF), protein solvent accessible surface area (SASA) and radius of gyration (Rg) using Visual Molecular Dynamics (VMD) software [51] to verify the stability of the systems.

2.6. Binding free energy calculations

The Molecular Mechanics-Generalized Born Surface Area (MM-GBSA) approach approach included in AmberTools 22 software was used to determine the binding free energy [52,53]. This approach constitutes a decisive step in the evaluation of the structure and function of complexes, following a MD simulation. The binding free energy (ΔE_{bind}) was evaluated determined according to the following equations:

$$\Delta E_{bind} = E_{complex} - (E_{receptor} + E_{ligand})$$

$$\Delta E_{bind} = \Delta E_{gas} + \Delta E_{sol} - T\Delta S$$

$$\Delta E_{gas} = \Delta E_{ele} + \Delta E_{vdw}$$

$$\Delta E_{sol} = \Delta E_{GB} + \Delta E_{SA}$$

Where $E_{complex}$ is the free energy of the protein-ligand complex, $E_{receptor}$, and E_{ligand} are the free energies in solution of the isolated protein and ligand, respectively. ΔE_{gas} represents the gas phase interaction energy between the protein and the ligand, which includes the interaction energies electrostatic (ΔE_{ele}), van der Waals (ΔE_{vdw}) and internal energies. ΔE_{sol} is the free energy of solvation estimated as the sum of the polar free energy of solvation (ΔE_{GB}) calculated with the generalized born model [54] and the non-polar free energy of solvation (ΔE_{SA}) obtained by fitting SASA [55]. $T\Delta S$ presents the entropy changes that can be estimated by a normal mode analysis on a set of conformational snapshots during the molecular dynamics process. Nevertheless, several researchers have reported that the lack of entropy evaluation is not critical for the calculation of MM-GBSA binding free energies for protein-ligand complexes [56–58]. For this reason, the entropy contribution $T\Delta S$ of all complexes was not calculated.

3. Results and discussions

3.1. Analysis of the binding modes of the flavonoids with SARS-CoV-2 (3CLpro, RBD) receptor

The computer-aided drug design (CADD) approach is a dynamic research area. Computational screening of compounds has been extensively employed in recent years, including screening, design, identification of new drugs against COVID-19 [59–61]. Therefore, we performed molecular docking of the studied ligands with SARS-CoV-2 receptors. Table 2 shows the results of the calculated binding affinities of each ligand with the two receptors.

Table 2
Binding affinity of SARS-CoV-2 3CLpro and RBD with Ligands.

Ligands	Binding Energy of SARS-CoV-2 3CLpro (kcal/mol)	Binding Energy of SARS-CoV-2 RBD (kcal/mol)
Herbacetin	−9.81	−8.03
Morin	−9.61	−8.46
Puerarin	−7.62	−5.72
Daidzein	−7.45	6.11
Silibinin	−9.59	−9.03
Tomentin A	−10.21	−9.51
Tomentin B	−10.02	−9.62
Tomentin C	−10.03	−8.92
Tomentin D	−9.23	−8.72
Tomentin E	−10.41	−8.32
3′-O-methyldiplacol	−9.18	−8.19
4′-O-methyldiplacol	−9.24	−8.39
3′-O-methyldiplacone	−9.08	−7.83
4′-O-methyldiplacone	−9.87	−8.51
Diplacone	−9.59	−8.19
Hesperetin	−8.06	−7.8
Hesperidin	−10.47	−9.38
Nobiletin	−7.47	−5.87
Galangin	−10.06	−7.87
amentoflavone	−12.43	−10.19
Bilobetin	−11	−8.89
Naringenin	−8.84	−7
Baicalein	−9.59	−8.19
Myricetin	−10.42	−8.66
Quercetin	−10.71	−8.26
kaempferol	−9.75	−7.69

For the binding site of SARS-CoV-2 3CLpro receptor, the binding affinity values range from −7.45 and −12.43 kcal/mol. The binding affinity values reveal strong competition for all ligands except for the ligands Puerarine, Daidzein, and Nobiletin. Thus, the ligand amentoflavone has a higher binding affinity (−12.43 kcal/mol), as well as the Tomentin A, Tomentin B, Tomentin C, Tomentin E, Hesperidin, Galangin, Bilobetin, Myricetin and Quercetin have a binding affinity higher than −10 kcal/mol, the other ligands vary between −8 and 10 kcal/mol with the exception of the Puerarin, Daidzein and Nobiletin which are lower than −8 kcal/mol. For the receptor binding site of SARS-CoV-2 DBR, the binding affinity values range from −5.72 to −10.19 kcal/mol. Thus, the ligand amentoflavone has a higher binding affinity (−10.19 kcal/mol). All ligands have binding affinity values greater than −8 kcal/mol, with the exception of Puerarin, Daidzein, 3′-O-methyldiplacone, Hesperetin, Nobiletin, Galangin, Naringenin and kaempferol ligands. From our docking analysis, almost all complexes have convergent complexation energy. To verify that these ligands from the flavonoid family are capable to be potential inhibitors of SARS-CoV-2, it is imperative to compare the binding site affinity with the best placement of the ligands in the active site of each receptor.

3.2. Interaction analysis of the ligands bound within binding pockets SARS-CoV-2 3CLpro and RBD

In order to analyze the mechanism of interactions between bioactive molecules and their respective enzymatic targets, the visualization of intermolecular interaction modes to predict biological activity was further analyzed. For the purpose of predicting the activity of SARS-CoV-2, the important sites in the case of 3CLpro of SARS-CoV-2 that formed the active site pocket are located at His41, Met49, Leu141, Asn142, Gly143, Ser144, Cys145, His163, His164, Met165, Glu166, Leu167, Asp187, Arg188, Gln189, Thr190 and Ala191. The recurrence of residues Asn142, Leu141, Ser144, and Cys145 indicates that they may be required for inhibitor binding [41]. The pocket that forms the SARCoV-2 RBD active site involved in ACE2 binding include Arg403, Asp405, Lys417, Gly446, Tyr449, Tyr453, Leu455, Phe456, Ala475, Phe486, Asn487, Tyr489, Gln493, Gly496, Gln498, Thr500, Asn501, Gly502 and Tyr505 with Gln24, His34, Glu35, Asp38, Tyr41, Gln42 and Lys353 in ACE2 [42,62].

The distances and angles, as well as the residues involved in the hydrogen bonds between the target protein and these ligands, have been grouped in Table 3. The 2D visualization of the best active compounds,

Table 3
Hydrogen bonding interactions (distances and angles) from molecular docking of SARS-CoV-2 3CLpro and RBD with the best ligands.

Ligand	SARS-CoV-2 3CLpro				Ligand	SARS-CoV-2 RBD			
	Residue groups	Ligand groups	distances (Å)	angles θ(°)		Residue groups	Ligand groups	distances (Å)	angles θ(°)
Silibinin	Asn142	H–O	2.14	100.819	Herbacetin	Asp38	H–O	3.01	100.739
	Ser144	H–O	2.92	133.411		Try453	O=C_2	1.93	137.418
	Cys145	H–O	3.07	92.489		Ser494	H–O	2.35	93.548
	Met165	H–O	2.49	109.103		Gly496	O–C	2.4	159.033
	Glu166	H–O	1.89	177.26		Asn501	H–O	1.96	122.375
	Gln192	H–O	2.6	103.613					
Tomentin A	Leu141	H–O	1.91	120.673	Morin	Glu406	H–O	2.38	155.738
	Asn142	H–O	2.84	104.353		Try453	H–O	2.71	116.802
	Asn142	H–O	3.03	92.387		Try453	H–O	1.8	140.465
	Gly143	H–O	2.39	104.216		Tyr505	H–O	2.04	121.609
	Ser144	O=C_2	2.13	120.685					
	Cys145	H–O	2.55	125.431					
Tomentin B	Leu141	H–O	1.88	145.814	Silibinin	Glu35	H–O	2.2	108.256
	Asn142	H–O	1.97	130.576		Glu35	H–O	1.65	118.008
	Gly143	H–O	2.84	104.357		Leu492	H–O	2.28	135.946
	Ser144	O=C_2	2.07	104.29		Gly496	O–C	1.93	154.117
	Cys145	H–O	2.37	115.492		Asn501	H–O	1.85	134.98
4′-O-methyldiplacone	Phe140	H–O	1.92	125.16	Tomentin E	Arg403	O–C	2.32	98.748
	Gly143	O=C2	2.39	114.769		Try453	O–C	1.81	110.699
	Ser144	O=C_2	2.33	136.801		Try453	H–O	2.26	133.48
	Ser144	O=C2	2.47	159.34		Ser494	H–O	2.33	151.52
	Cys145	O=C2	2.96	127.827		Tyr505	O–C	2.37	112.066
	Glu189	H–O	2.02	139.21					
Hesperidin	Leu141	H–O	2.95	100.203	amentoflavone	Asp405	H–O	1.91	137.377
	Ser144	O=C_2	1.95	124.232		Asp405	H–O	2.4	141.089
	Ser144	O=C_2	1.52	145.131		Glu406	H–O	3.06	105.893
	Cys145	O=C_2	2.54	108.624		Try453	H–O	1.98	164.01
	Glu166	H–O	2.22	130.024		Tyr505	H–O	1.92	133.954
	Glu166	H–O	1.86	146.064					
	Glu166	H–O	1.98	133.452					
Amentoflavone	Cys145	H–O	2.63	147.632	Bilobetin	Glu35	H–O	2.65	93.156
	His164	H–O	2	128.545		Asp38	H–O	1.75	125.652
	Leu167	H–O	2.03	168.13		Try453	H–O	1.96	120.927
	Thr190	H–O	2.34	146.181		Asn501	H–O	2.16	132.582
						Tyr505	H–O	1.73	146.577
Bilobetin	Phe140	H–O	2.39	109.977	Baicalein	Lys353	O=C_2	1.76	103.952
	Gly143	O=C2	2.65	142.871		Asn501	H–O	1.77	155.702
	Cys145	O=C2	2.87	138.296		Asn501	H–O	1.67	153.704
	Glu166	O–C	2.74	146.766		Tyr505	H–O	1.9	172.909
	Glu166	H–O	2.83	111.691					
	Arg188	H–O	2.08	109.425					
	Gln189	H–O	2.76	119.617					
					Quercetin	Lys353	H–O	1.9	132.03
						Glu406	H–O	2.02	135.391
						Asn501	H–O	2.04	160.539
						Asn501	H–O	1.81	149.349

based on the number of hydrogen bonds with the important amino acids of the 3CLpro and RBD active sites of SARS-CoV-2, were presented in Figs. 1 and 2, respectively. Fig. 1 shows that Silibinin, Tomentin A, Tomentin B, 4′-O-methyldiplacone, Hesperidin, Amentoflavone and Bilobetin formed several hydrogen bonding interactions with the residues Asn142, Leu141, Ser144 and Cys145 in the deepest regions of the SARS-CoV-2 3CLpro active site. As a result, they are able to cover the receptor binding pocket of this protein, which prevents COVID-19 replication and transcription. Furthermore, we observed a strong correlation between the best interactions formed with SARS-CoV-2 3CLpro and the high docking score observed for these compounds. However, the high docking score does not reflect the position and formation of strong interactions with the active site of SARS-CoV-2 3CLpro. These results indicate that these ligands could be studied as a potential therapeutic solution against COVID-19 by inhibiting virus replication and transcription. Furthermore, Fig. 2 revealed that Herbacetin, Morin, Silibinin, Tomentin E, Amentoflavone, Bilobetin, Baicalein and Quercetin established several hydrogen bonding interactions with the target protein (Table 3). These hydrogen bonding interactions with Arg403, Tyr449, Gly496, Gln498 and Asn501 are the most favourable positions in the SARS-CoV-2 RBD active site compared to the other compounds studied. The selected ligands were those with the best docking score, but several complexes with the highest docking score did not form strong interactions with the SARS-CoV-2 RBD active site. Thus, the position and stability of ligands in the active site play a decisive role in confirming the potential therapeutic pathway for COVID-19. Based on these results, these ligands are capable to establish several hydrogen bond interactions with the main residues. Therefore, they are theoretically capable to bind to the pocket formed by the SARS-CoV-2 protein residues and interfering with the function of the virus, indicating the potential of these compounds as SARS-CoV-2 inhibitors with similar binding sites and pocket structures. Thus, the molecular docking results

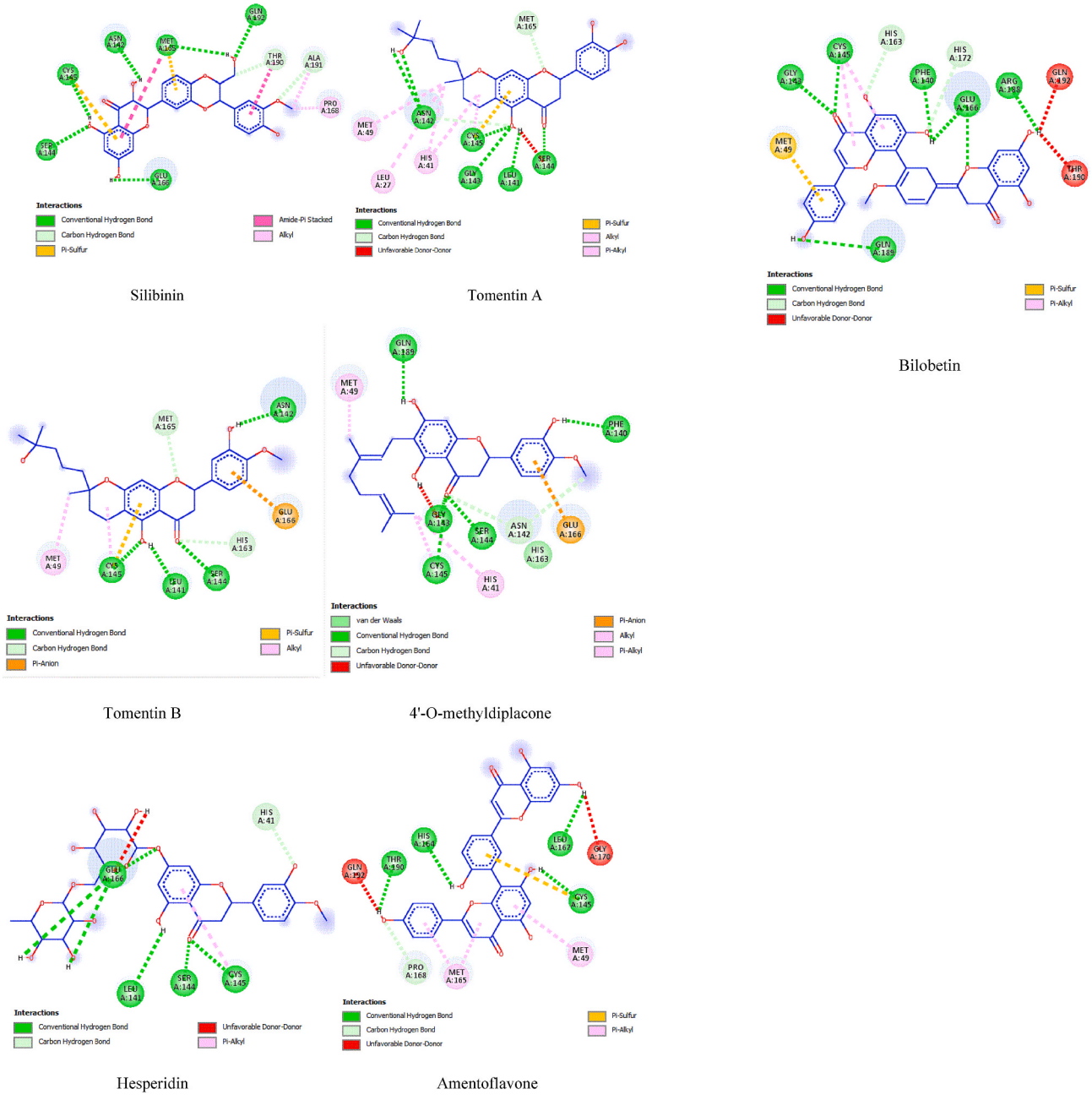

Fig. 1. 2D visualization of the interaction types between the best ligands with SARS-CoV-2 3CLpro.

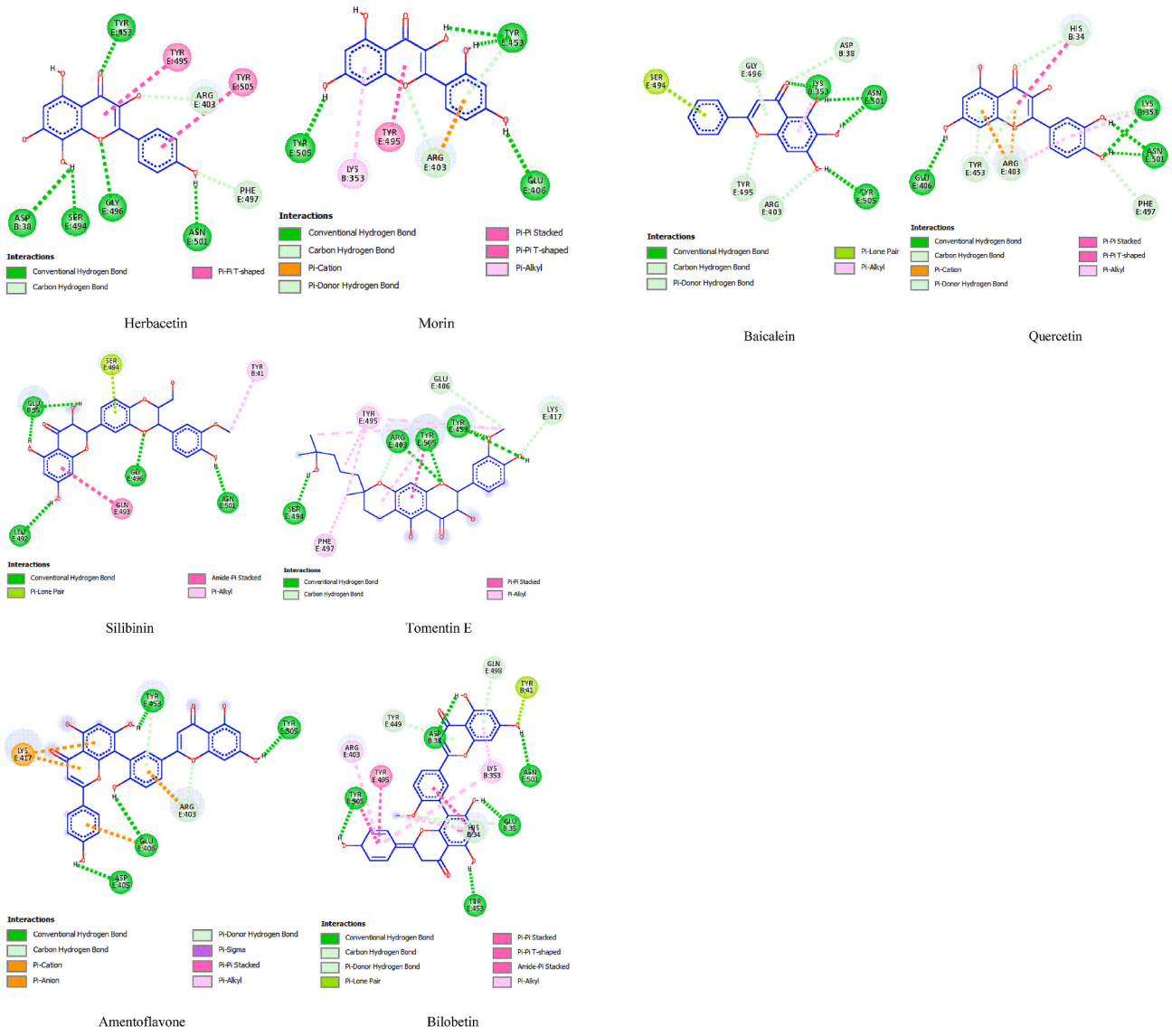

Fig. 2. 2D visualization of the interaction types between the best ligands with SARS-CoV-2 RBD.

also showed that silibinin, Amentoflavone and Bilobetin could inhibit both sites of SARS-CoV-2, thus these compounds could be effective inhibitors for COVID-19. Furthermore, modeling of the contact areas between the ligands and the receptor shows that these complexes are mainly stabilized by hydrogen bonds involving the O–H and C=O groups where the ligand can act simultaneously as a donor and acceptor with the residues, which are essential for SARS-CoV-2 inhibition.

3.3. Docking validation protocol

To validate the accuracy of the docking procedure for predicting the conformation of the ligand bound to the receptor, we performed a new docking of the native ligand with the SARS-CoV-2 3CLpro receptor. Fig. 3 shows the superimposed view between the docked ligand and the co-crystallized native ligand. Several studies have shown that RMSD is not a good parameter for docking validation [63–65], because RMSD suffers from serious problems when it comes to large, nearly symmetrical molecules and does not provide any information about the quality of the complex representation as well as ligand-receptor interactions. In this study, we rely on a new docking validation method called visual inspection. Fig. 4 shows the 2D and 3D visualization of the interactions of the docked ligand and the co-crystallized native ligand with the

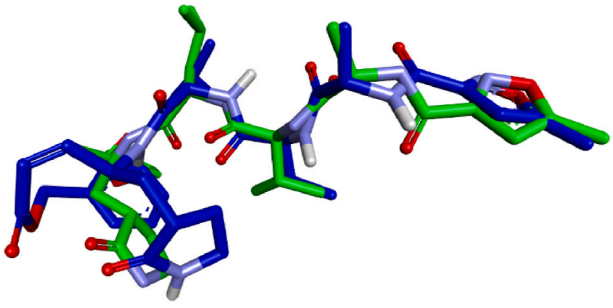

Fig. 3. The visualization of the superposition the ligand position based on the re-docking process of the crystallographic ligand (green = original, blue = docked). (For interpretation of the references to colour in this figure legend, the reader is referred to the Web version of this article.)

SARS-CoV-2 3CLpro protein.

The results of this visual inspection of the re-docking ligand clearly show that the docked ligand formed approximately the same interaction modes with the same amino acids at the active site of the SARS-CoV-2 3CLpro, compared to the crystallized ligand. Based on these results, it

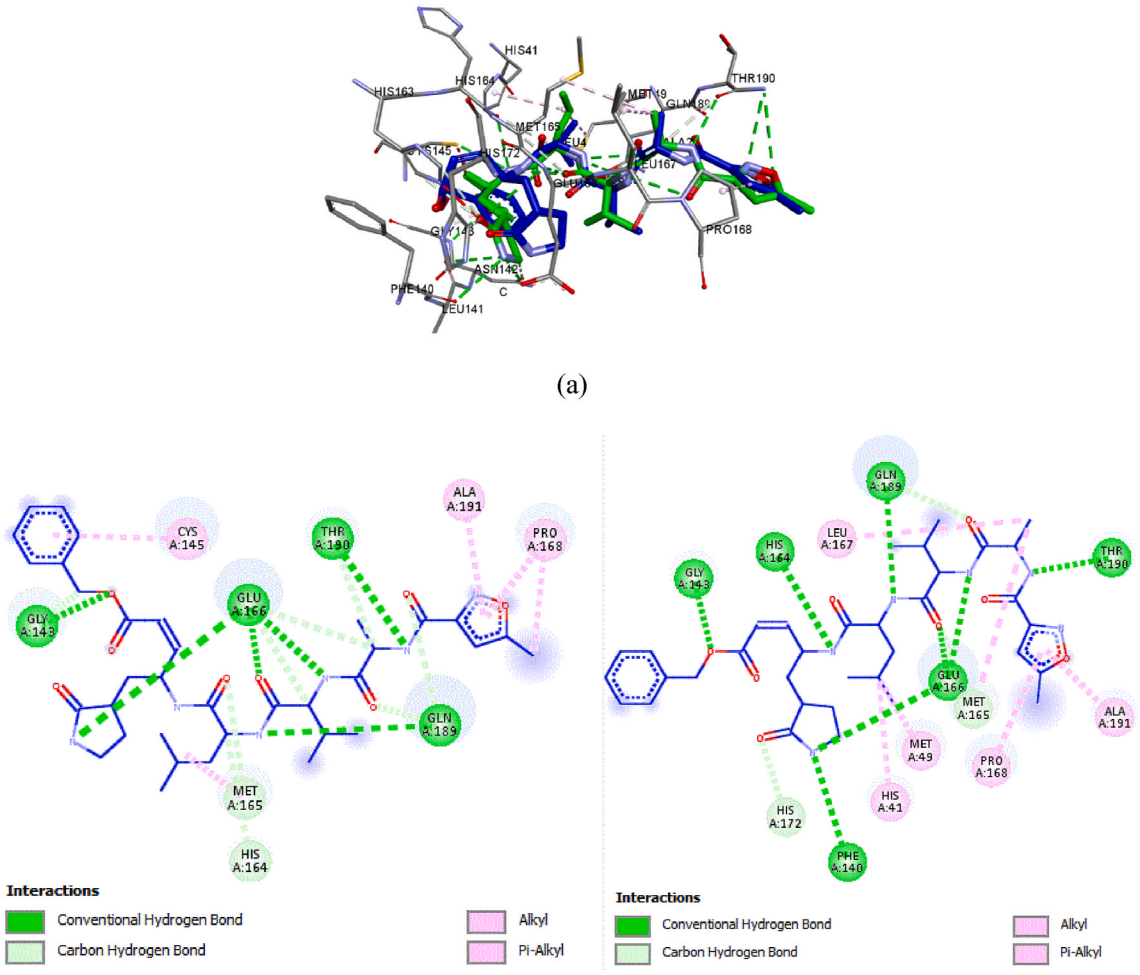

Fig. 4. (a) 3D visualization comparison between ligand pose prediction results and the crystallographic ligand pose. (b) 2D visualization showing interactions of ligand pose prediction result. (c) 2D visualization showing interactions of the crystallographic ligand pose.

can be concluded that the use of visual inspection as a new method for validating molecular docking yields convincing results, and that the docking process was successfully validated by the visual inspection method.

3.4. ADMET prediction and drug-likeness

To ensure that the best bioactive compounds against COVID-19 can be viable drugs, we used ADMET pharmacokinetic parameters and druglikeness. Table 4 presents the in silico prediction of ADMET properties using the online tool pkCSM. Table 5 presents the in silico prediction of druglikeness properties using the SwissADME online tool [66,67].

Overall, an absorption value less than 30% means poor absorption. The above results show that all compounds have good absorption in the human intestine, except for Hesperidin, which has an absorption value of less than 30%. In addition, the Volume of distribution (VDss) is estimated to be high if the value is greater than 0.45. Blood brain barrier (BBB) and central nervous system (CNS) permeability standard values (>0.3 to < -1 Log BB and >-2 to < -3 LogPS), respectively. For a particular compound a LogBB < -1 is poorly distributed in the brain, whereas LogBB >0.3 is potential to cross the BBB and LogPS > -2 considered to penetrate the CNS, whereas LogPS < −3 is difficult to move in the CNS. The results indicate that all ligands, except Amentoflavone and Bilobetin, have an increased ability to cross barriers.

Drug metabolism is the term used to describe the biotransformation of pharmaceutical substances in the body. Drugs produce several enzymatic metabolites, and each metabolite formed has different pharmacological, pharmacokinetic and physico-chemical propertiesIt is therefore essential to consider drug metabolism and interactions with other drugs. Cytochrome P450 inhibition, including CYP: 1A2, 2C19, 2C9, 2D6, and 3A4, plays a major role in drug metabolism, as it causes drug interactions and some cytochromes P450 can be considered as therapeutic targets. Several studies have shown that drugs such as lopinavir/ritonavir and hydroxychloroquine sulfate, which they have shown their effectiveness in the treatment of COVID-19 patients, have potent inhibitory effects on CYP3A4 and CYP2D6 [68,69]. The compounds Herbacetin, Morin, Tomentin A, Tomentin B, 4′-O-methyldiplacone and Quercetin were found to be inhibitors of the enzymes CYP3A4 and CYP2D6. Clearance is a constant that describes the relationship between the rate of drug clearance and the concentration of drug in the body. Therefore, a low clearance value indicates increased persistence of drugs in the body. The all compounds show a good persistence of the drug in the body. Furthermore, it is necessary to verify that the predicted compounds are non-toxic. The all compounds presented are non-toxic. According to these criteria, the compounds Herbacetin, Morin, Tomentin A, Tomentin B, 4′-O-methyldiplacone and Quercetin have good pharmacokinetic properties.

The drug-likeness results show that the compounds Herbacetin, Morin, Tomentin A, Tomentin B, Tomentin B, 4′-O-methyldiplacone,

Table 4
In silico ADMET prediction of the potential inhibitors.

Compounds	Absorption	Distribution			Metabolism						Excretion	Toxicity
	Intestinal absorption (human)	VDss (human)	BBB permeability	CNS permeability	Substrate		Inhibitor				Total Clearance	AMES toxicity
					CYP 2D6	CYP 3A4	CYP 1A2	CYP 2C19	CYP 2C9	CYP 2D6	CYP 3A4	
	Numeric (% Absorbed)	Numeric (Log L/kg)	Numeric (Log BB)	Numeric (Log PS)	Categorical (Yes/No)						Numeric (Log ml/min/kg)	Categorical (Yes/No)
Herbacetin	68	1.323	−1.297	−3.12	No	No	Yes	No	No	Yes	Yes	0.374	No
Morin	75.408	1.229	−1.18	−3.389	No	No	Yes	No	No	Yes	Yes	0.486	No
Silibinin	92.517	0.024	−1.738	−3.792	No	Yes	No	No	Yes	No	No	0.018	No
Tomentin A	81.796	0.382	−1.418	−3.059	No	Yes	No	No	Yes	No	Yes	0.031	No
Tomentin B	86.48	0.482	−1.271	−2.962	No	Yes	No	Yes	Yes	No	Yes	0.102	No
Tomentin E	74.135	0.451	−1.502	−3.223	No	Yes	No	Yes	Yes	No	No	0.104	No
4′-O-methyldiplacone	87.132	0.409	−1.142	−2.775	No	Yes	No	Yes	Yes	No	Yes	0.448	No
Hesperidin	23.656	0.231	−1.828	−5.022	No	Yes	No	No	No	No	No	0.324	No
amentoflavone	88.044	−1.159	−2.239	−3.107	No	No	No	No	No	No	No	0.581	No
Bilobetin	85.455	−1.139	−2.169	−3.244	No	No	No	No	No	No	No	0.67	No
Baicalein	95.472	−0.506	−1.219	−2.296	No	No	Yes	Yes	Yes	No	No	0.252	No
Quercetin	77.207	1.559	−1.098	−3.065	No	No	Yes	No	No	Yes	Yes	0.407	No

Table 5
Drug likeness prediction of the potential inhibitors based on the rules of Lipinski, Ghose, Veber, Egan and Muegge.

Compounds	Druglikeness				
	Lipinski	Ghose	Veber	Egan	Muegge
Herbacetin	Yes	Yes	Yes	Yes	Yes
Morin	Yes	Yes	Yes	Yes	Yes
Silibinin	Yes	No	No	No	No
Tomentin A	Yes	Yes	Yes	Yes	Yes
Tomentin B	Yes	Yes	Yes	Yes	Yes
Tomentin E	Yes	Yes	Yes	Yes	Yes
4′-O-methyldiplacone	Yes	Yes	Yes	Yes	No
Hesperidin	No	No	No	No	No
amentoflavone	No	No	No	No	No
Bilobetin	Yes	No	No	No	No
Baicalein	Yes	Yes	Yes	Yes	Yes
Quercetin	Yes	Yes	Yes	Yes	Yes

Baicalein and Quercetin are in perfect agreement with all drug similarity rules (Table 5). Based on these results, it can be concluded that the compounds Herbacetin, Morin, Tomentin A, Tomentin B, 4′-O-methyldiplacone and Quercetin have the potential to become excellent drug candidates against COVID-19.

3.5. Molecular dynamics analysis

After the analysis of molecular docking and ADMET properties of the predicted compounds, MD studies of the compounds Tomentin A, Tomentin B and 4′-O-methyldiplaconewith SARS-CoV-2 3CLpro active site as well as the compounds Herbacetin, Morin and Quercetin with SARS-CoV-2 RBD active site were performed, using RMSD and RMSF parameters to analyze the dynamic behaviour and stability of the target protein. The RMSD, RMSF, SASA and R(g) plots of the SARS-CoV-2 3CLpro and RBD complexes with the best predicted compounds are shown in Fig. 5, Fig. 6, Fig. 7 and Fig. 8, respectively.

In the case of SARS-CoV-2 3CLpro (Fig. 5a), analysis of the RMSD plots indicates that all systems showed a rapid increase in RMSD values from 0.6 Å to 1.3 Å within a 20 ns period. Thereafter, all systems fluctuated within a similar distance range of 1.3 Å and 1.5 Å, implying that all systems reached a steady state and equilibrium. The RMSD values of Tomentin A, Tomentin B and 4′-O-methyldiplacone complexed with the SARS-CoV-2 3CLpro were 1.644 Å, 1.681 Å and 1.629 Å, respectively. According to the study by Beura et al. [70], an RMSD value of less than 3 Å is an indicator of the conformational stability of protein-ligand complexes. All compounds have a value below 1.7 Å. Thus, all compounds are stable in the active sites of the proteins and the ligand 4′-O-methyldiplacone has the best stability. In the case of SARS-CoV-2 RBD (Fig. 5b), analysis of the RMSD plots indicates that all systems showed a rapid increase in RMSD values from 0.6 Å to 1.4 Å within a 20 ns period. Subsequently, all systems fluctuated within a similar distance range of 1.4 Å and 1.7 Å, implying that all systems reached a steady state and equilibrium. From the RMSD plot, the RMSD values of the compounds Herbacetin, Morin and Quercetin complexed with the SARS-CoV-2 RBD protein were 1.704 Å, 1.823 Å and 2.153 Å, respectively, with RMSD values less than 2.2 Å indicating that all compounds are stable in the active site of the SARS-CoV-2 RBD protein and the compound Herbacetin is the most stable. The RMSF trajectories measure the ligand binding affects the flexibility of the protein during the 100 ns MD simulation, which is crucial information on the receptor's stability, stiffness and compactness. A high RMSF value indicates that the residue is flexible, while a low RMSF value indicates that the residue is stable. In the case of SARS-CoV-2 3CLpro (Fig. 6a), most residues share the same RMSF values, with larger fluctuations present in different ranges, such as Ser1 (3.971 Å), Asn277 (1.704 Å), Gly302 (2.151 Å) and Gln306 (2.751 Å), these residues are not involved as they are located in the inactive regions of the SARS-CoV-2 3CLpro protein. However, the crucial active

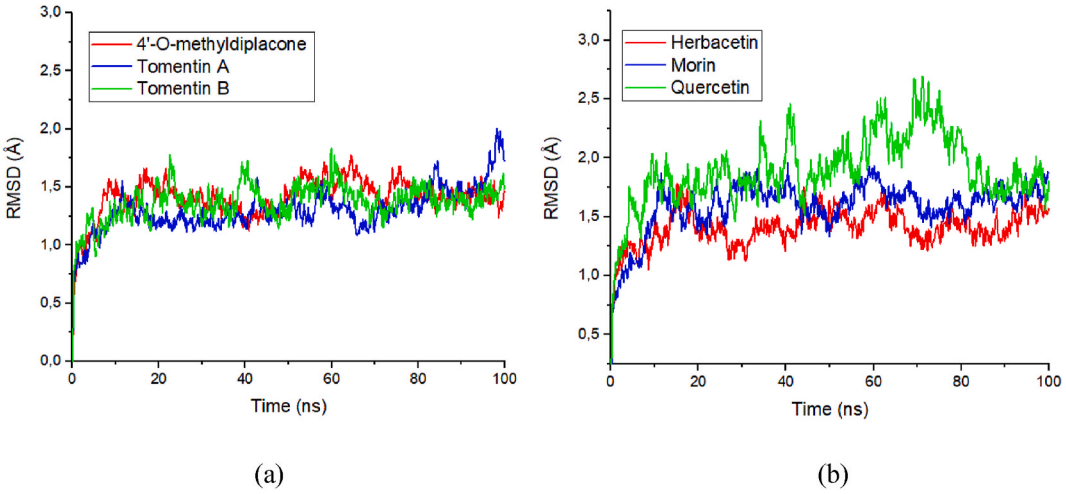

(a) (b)

Fig. 5. a) The RMSD values of SARS-CoV-2 3CLpro in complex with the corresponding ligands. b) The RMSD values of SARS-CoV-2 RBD in complex with the corresponding ligands.

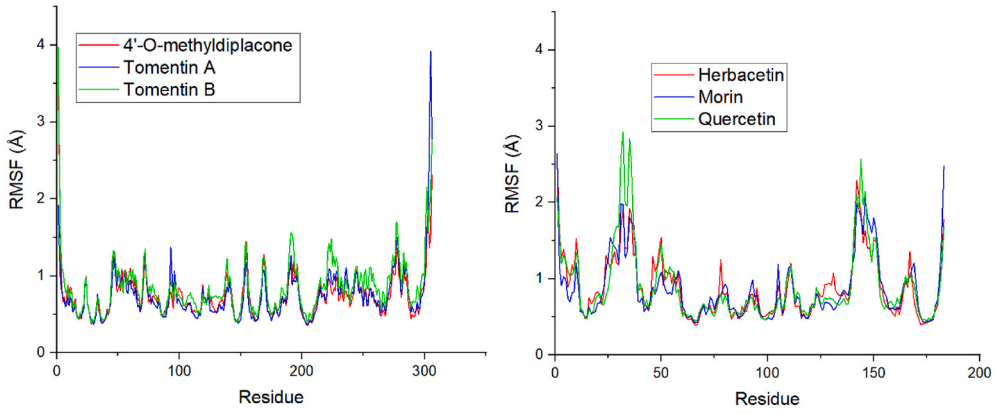

(a) (b)

Fig. 6. a) The RMSF values of SARS-CoV-2 3CLpro residues in complex with the corresponding ligands. b) The RMSF values of SARS-CoV-2 RBD residues in complex with the corresponding ligands.

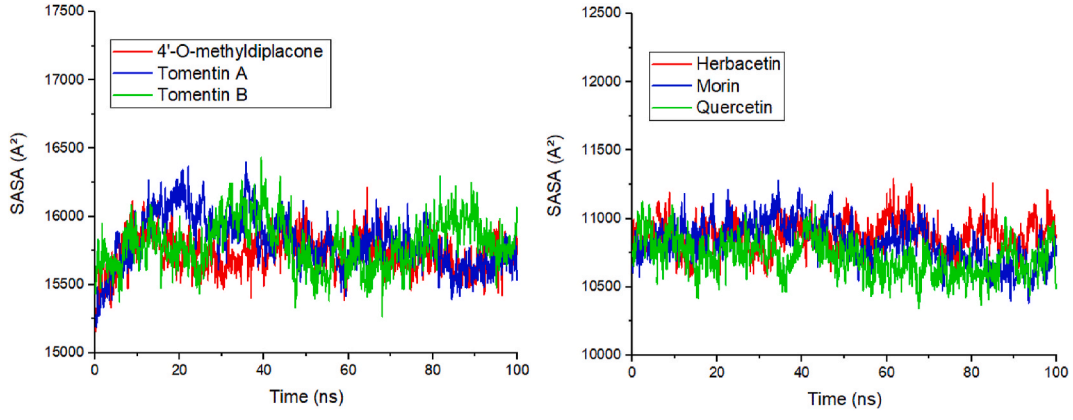

(a) (b)

Fig. 7. a) SASA values of SARS-CoV-2 3CLpro in complex with the corresponding ligands. b) SASA values of SARS-CoV-2 RBD in complex with the corresponding ligands.

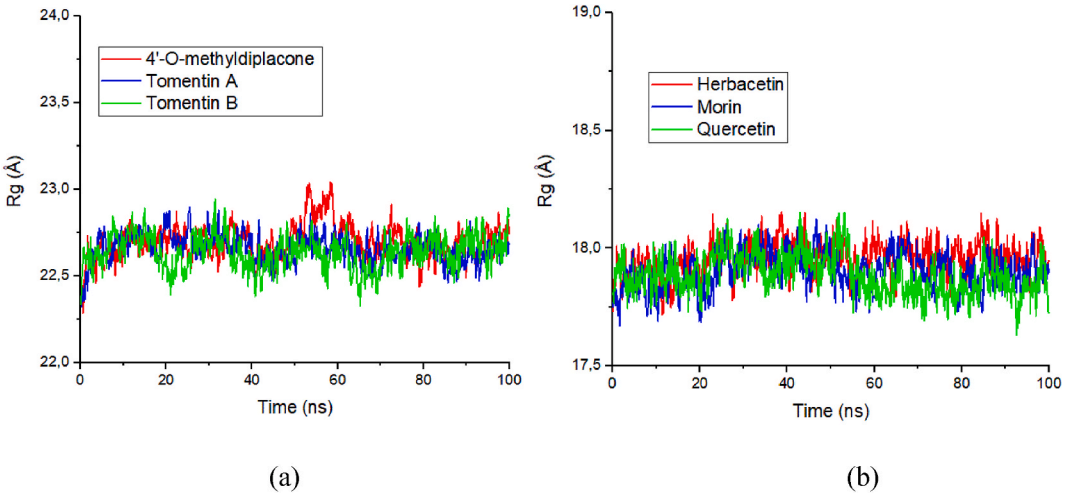

Fig. 8. a) Radius of gyration (Rg) values of SARS-CoV-2 3CLpro in complex with the corresponding ligands. b) Radius of gyration (Rg) values of SARS-CoV-2 RBD in complex with the corresponding ligands.

site residues, such as Asn142, Leu141, Ser144, and Cys145, show smaller fluctuations with RMSF values below 0.8 Å, indicating that the established hydrogen bonds stabilize the ligands with the SARS-CoV-2 3CLpro protein. In the case of the SARS-CoV-2 RBD (Fig. 6b), residues with larger fluctuations, such as Cys336 (2.636 Å), Val367 (2.924 Å), Asn370 (2.835 Å) and Pro479 (2.566 Å), are not involved in the active site, but crucial active site residues such as Arg403, Glu406, Try453, Gly496, Asn501 and Tyr505 show smaller fluctuations with RMSF values below 1 Å, indicating that established hydrogen bonds stabilize the ligand complexation with the SARS-CoV-2 RBD protein. These data confirm the RMSD results that all predicted ligand complexation with SARS-CoV-2 3CLpro and RBD protein exhibit greater conformational stability.

The solvent accessible surface area (SASA) calculates the surface area of a protein-ligand complex that can interact with solvent molecules. Decreasing SASA values of a protein indicate an increase in the compactness of the protein and less exposure to solvents. In the case of SARS-CoV-2 3CLpro (Fig. 7 a), the SASA values are similar for all three complexes, there is a slight tolerable increase in the 20 ns period but in general the SASA values remain almost stable, this result indicates that all complexes are compact. In the case of SARS-CoV-2 RBD (Fig. 7b), low SASA values for all three complexes was observed with significant stabilization throughout the simulations. This indicates that there is no change in the structure of the complex, and on the other hand, a high compactness of the complex. In general, the SASA results suggest the formation of stable complexes for both proteins with the corresponding ligands.

The radius of gyration (Rg) provides an indicator of the level of compactness of protein-ligand complexes. There is an inverse relationship between Rg values and protein compactness. As shown in Fig. 8 a, a slight tolerable increase in the 10 ns period for all three complexes, thereafter all systems have smaller and stable fluctuations in Rg value. As shown in Fig. 8 b, the structures of the three complexes show relatively little variation in Rg values throughout the simulations, implying that none of the systems underwent significant conformational changes. Therefore, it can be concluded that all systems were stable and compact. In general, it can be concluded that the docking results of all predicted ligand complexation with the SARS-CoV-2 3CLpro and RBD protein show greater conformational stability.

3.6. Binding free energy calculations

The binding free energy calculations for the six complexes based on the MD trajectory were performed using the MM-GBSA method are listed in Table 6.

For all complexes, the ΔE_{gas} and ΔE_{sol} values are negative and positive, indicating a favourable and an unfavourable energy contribution to the overall binding free energy, respectively. In the case of the SARS-CoV-2 3CLpro, the binding free energy (ΔE_{bind}) values of compounds Tomentin A, Tomentin B and 4′-O-methyldiplacone were −23.426, −16.221and −34.119 kcal mol−1, respectively. Compound 4′-O-methyldiplacone seems to be the most active among the three designed inhibitors with binding free energy (−34.119 kcal mol-1) for SARS-CoV-2 3CLpro. In the case of the SARS-CoV-2 RBD, the ΔE_{bind} values of compounds Herbacetin, Morin and Quercetin were −28.207, −19.216 and −1.724 kcal mol−1, respectively. The compound Herbacetin was found to be the most active of the three designed inhibitors with a binding free energy of −28.207 kcal mol-1 for SARS-CoV-2 RBD. The ΔE_{bind} values of all designed inhibitors are all more negative, except of the compound Quercetin, indicating the most energetically favourable, theoretically active and significant for the experimental tests. Moreover, the MM-GBSA results are fully consistent with the molecular dynamics results, as a correlation was observed between the binding free energy values and the RMSD values. The results of this study could represent excellent

Table 6
The binding free energy details of the SARS-CoV-2 3CLpro and RBD in complex with the selected ligand.

Energy Parameter (kcal/mol)	SARS-CoV-2 3CLpro			SARS-CoV-2 RBD		
	Tomentin A	Tomentin B	4′-O-methyldiplacone	Herbacetin	Morin	Quercetin
ΔE_{vdw}	−30.470	−27.921	−43.290	−33.762	−26.927	−13.546
ΔE_{ele}	−20.452	−16.379	−22.803	−38.692	−22.810	−30.441
ΔE_{GB}	31.614	31.910	37.552	49.642	36.634	43.563
ΔE_{SA}	−4.117	−3.830	−5.578	−3.662	−2.997	−3.512
ΔE_{gas}	−50.922	−44.301	−66.093	−74.187	−52.852	−41.776
ΔE_{sol}	27.496	28.079	31.974	45.979	33.636	40.051
ΔE_{bind}	−23.426	−16.221	−34.119	−28.207	−19.216	−1.724

candidates for the treatment of COVID-19.

4. Conclusion

Inhibition of SARS-CoV-2 3CLpro and RBD sites is an important target for treating COVID-19. In this study, we identified some drug candidates against COVID-19 from a set of 26 studied compounds belonging to the flavonoid family, using molecular docking, ADMET properties, drug-likeness and molecular dynamics simulations. Molecular docking revealed that the ligands (Silibinin, Tomentin A, Tomentin B, 4′-O-methyldiplacone, Hesperidin, Amentoflavone, Bilobetin) as well as (Herbacetin, Morin, Silibinin, Tomentin E, Amentoflavone, Bilobetin, Baicalein, Quercetin) showed inhibitory potential for SARS-CoV-2 3CLpro and RBD, respectively. Thus, Silibinin, Amentoflavone and Bilobetin presented potential inhibitory for the SARS-CoV-2 3CLpro and RBD receptors. The molecular docking results were tested with a new validation method based on visual inspection. The evaluation of ADMET pharmacokinetic properties and the drug likeness in silico of the best compounds revealed that Herbacetin, Morin, Tomentin A, Tomentin B and Quercetin could be effective against COVID-19. Subsequently, the compounds with the best pharmacokinetic properties were selected for further analysis using molecular dynamics studies. The molecular dynamics results demonstrated the accurate docking of best compounds in terms of reliability and stability. Furthermore, the MM-GBSA results indicate strong binding energies between the ligands and the receptor, which also confirms our docking results. These results hold great promise in halting the progression of the COVID-19 pandemic.

Declaration of competing interest

The authors declare that there are no conflicts of interest regarding the publication of this paper.

Acknowledgements

This research was supported by the grant programme for scientific and technological research in connection with “COVID-19 of National Center for Scientific and Technical Research (CNRST) and Sidi Mohamed ben Abdellah University (USMBA). Grant number: Cov/2020/54 and the project name is " COV19Sim Maroc".

References

[1] N. Srivastava, P. Baxi, R.K. Ratho, S.K. Saxena, in: Global Trends in Epidemiology of Coronavirus Disease 2019 (COVID-19), Springer, Singapore, 2020, pp. 9–21, https://doi.org/10.1007/978-981-15-4814-7_2.

[2] Y.C. Wu, C.S. Chen, Y.J. Chan, The outbreak of COVID-19: an overview, J. Chin. Med. Assoc. 83 (2020) 217–220, https://doi.org/10.1097/JCMA.0000000000000270.

[3] R.T. Butt, O.S. Janjua, S.M. Qureshi, M.S. Shaikh, J. Guerrero-Gironés, F. J. Rodríguez-Lozano, M.S. Zafar, Dental healthcare amid the COVID-19 pandemic, Int. J. Environ. Res. Publ. Health 18 (2021), 11008, https://doi.org/10.3390/IJERPH182111008, 11008. 18 (2021).

[4] B.S. Bleier, M. Ramanathan, A.P. Lane, COVID-19 vaccines may not prevent nasal SARS-CoV-2 infection and asymptomatic transmission, Otolaryngol. Head Neck Surg. 164 (2021) 305–307, https://doi.org/10.1177/0194599820982633.

[5] A. Christie, J.T. Brooks, L.A. Hicks, E.K. Sauber-Schatz, J.S. Yoder, M.A. Honein, Guidance for implementing COVID-19 prevention strategies in the Context of varying community transmission levels and Vaccination Coverage, Morb. Mortal. Wkly. Rep. 70 (2021) 1047, https://doi.org/10.15585/MMWR.MM7030E2.

[6] H. Zhang, J.M. Penninger, Y. Li, N. Zhong, A.S. Slutsky, Angiotensin-converting enzyme 2 (ACE2) as a SARS-CoV-2 receptor: molecular mechanisms and potential therapeutic target, Intensive Care Med. 46 (2020) 586–590, https://doi.org/10.1007/s00134-020-05985-9.

[7] L. Premkumar, B. Segovia-Chumbez, R. Jadi, D.R. Martinez, R. Raut, A. J. Markmann, C. Cornaby, L. Bartelt, S. Weiss, Y. Park, C.E. Edwards, E. Weimer, E. M. Scherer, N. Rouphael, S. Edupuganti, D. Weiskopf, L.V. Tse, Y.J. Hou, D. Margolis, A. Sette, M.H. Collins, J. Schmitz, R.S. Baric, A.M. de Silva, The receptor-binding domain of the viral spike protein is an immunodominant and highly specific target of antibodies in SARS-CoV-2 patients, Sci. Immunol. 5 (2020), https://doi.org/10.1126/SCIIMMUNOL.ABC8413.

[8] S. Gildenhuys, Expanding our understanding of the role polyprotein conformation plays in the coronavirus life cycle, Biochem. J. 477 (2020) 1479–1482, https://doi.org/10.1042/BCJ20200223.

[9] G. Li, Y. Fan, Y. Lai, T. Han, Z. Li, P. Zhou, P. Pan, W. Wang, D. Hu, X. Liu, Q. Zhang, J. Wu, Coronavirus infections and immune responses, J. Med. Virol. 92 (2020) 424–432, https://doi.org/10.1002/jmv.25685.

[10] J. Shang, Y. Wan, C. Liu, B. Yount, K. Gully, Y. Yang, A. Auerbach, G. Peng, R. Baric, F. Li, Structure of mouse coronavirus spike protein complexed with receptor reveals mechanism for viral entry, PLoS Pathog. 16 (2020), e1008392, https://doi.org/10.1371/journal.ppat.1008392.

[11] E. Procko, The sequence of human ACE2 is suboptimal for binding the S spike protein of SARS coronavirus 2, bioRxiv (2020), https://doi.org/10.1101/2020.03.16.994236.

[12] V. Monteil, H. Kwon, P. Prado, A. Hagelkrüys, R.A. Wimmer, M. Stahl, A. Leopoldi, E. Garreta, C. Hurtado del Pozo, F. Prosper, J.P. Romero, G. Wirnsberger, H. Zhang, A.S. Slutsky, R. Conder, N. Montserrat, A. Mirazimi, J.M. Penninger, Inhibition of SARS-CoV-2 infections in engineered human tissues using clinical-grade soluble human ACE2, Cell 181 (2020) 905–913, https://doi.org/10.1016/j.cell.2020.04.004, e7.

[13] E. Lautié, O. Russo, P. Ducrot, J.A. Boutin, Unraveling plant natural chemical diversity for drug discovery purposes, Front. Pharmacol. 11 (2020) 1, https://doi.org/10.3389/fphar.2020.00397.

[14] A.C. Shukla, The herbal drugs, in: Adv. Pharm. Biotechnol. Recent Prog. Futur. Appl., Springer Singapore, 2020, pp. 69–75, https://doi.org/10.1007/978-981-15-2195-9_6.

[15] S. Khaerunnisa, H. Kurniawan, R. Awaluddin, S. Suhartati, S. Soetjipto, Potential Inhibitor of COVID-19 Main Protease (M Pro) from Several Medicinal Plant Compounds by Molecular Docking Study, 2020, https://doi.org/10.20944/preprints202003.0226.v1.

[16] D. Dwarka, C. Agoni, J.J. Mellem, M.E. Soliman, H. Baijnath, Identification of potential SARS-CoV-2 inhibitors from South African medicinal plant extracts using molecular modelling approaches, South Afr. J. Bot. 133 (2020) 273–284, https://doi.org/10.1016/j.sajb.2020.07.035.

[17] S. Chtita, A. Belhassan, M. Bakhouch, A.I. Taourati, A. Aouidate, S. Belaidi, M. Moutaabbid, S. Belaaouad, M. Bouachrine, T. Lakhlifi, QSAR study of unsymmetrical aromatic disulfides as potent avian SARS-CoV main protease inhibitors using quantum chemical descriptors and statistical methods, Chemometr. Intell. Lab. Syst. 210 (2021), 104266, https://doi.org/10.1016/j.chemolab.2021.104266.

[18] S. Sarvagalla, S.B. Syed, M.S. Coumar, An overview of computational methods, tools, servers, and databases for drug repurposing, in: Silico Drug Des., Elsevier, 2019, pp. 743–780, https://doi.org/10.1016/b978-0-12-816125-8.00025-0.

[19] H. Hadni, M. Bakhouch, M. Elhallaoui, 3D-QSAR, Molecular Docking, DFT and ADMET Studies on Quinazoline Derivatives to Explore Novel DHFR Inhibitors, 2021, https://doi.org/10.1080/07391102.2021.2004233.

[20] A.V.B. Reddy, M. Moniruzzaman, V. Madhavi, J. Jaafar, Recent improvements in the extraction, cleanup and quantification of bioactive flavonoids, in: Stud. Nat. Prod. Chem., Elsevier B.V., 2020, pp. 197–223, https://doi.org/10.1016/B978-0-12-817907-9.00008-8.

[21] N.L. Allinger, Conformational analysis. 130. MM2. A hydrocarbon force field utilizing V1and V2Torsional Terms1,2, J. Am. Chem. Soc. 99 (1977) 8127–8134, https://doi.org/10.1021/ja00467a001.

[22] C. Veeramani, M.A. Alsaif, K.S. Al-Numair, Herbacetin, a flaxseed flavonoid, ameliorates high percent dietary fat induced insulin resistance and lipid accumulation through the regulation of hepatic lipid metabolizing and lipid-regulating enzymes, Chem. Biol. Interact. 288 (2018) 49–56, https://doi.org/10.1016/j.cbi.2018.04.009.

[23] J. Venu Gopal, Morin Hydrate, Botanical origin, pharmacological activity and its applications: a mini-review, Pharm. J. 5 (2013) 123–126, https://doi.org/10.1016/j.phcgj.2013.04.006.

[24] H.D. Gravina, N.F. Tafuri, A. Silva Júnior, J.L.R. Fietto, T.T. Oliveira, M.A.N. Diaz, M.R. Almeida, In vitro assessment of the antiviral potential of trans-cinnamic acid, quercetin and morin against equid herpesvirus 1, Res. Vet. Sci. 91 (2011) e158–e162, https://doi.org/10.1016/j.rvsc.2010.11.010.

[25] Y.-X. Zhou, H. Zhang, C. Peng, Puerarin: a review of pharmacological effects, Phyther. Res. 28 (2014) 961–975, https://doi.org/10.1002/ptr.5083.

[26] M.M. Alshehri, J. Sharifi-Rad, J. Herrera-Bravo, E.L. Jara, L.A. Salazar, D. Kregiel, Y. Uprety, M. Akram, M. Iqbal, M. Martorell, M. Torrens-Mas, D.G. Pons, S. D. Daştan, N. Cruz-Martins, F.A. Ozdemir, M. Kumar, W.C. Cho, Therapeutic potential of isoflavones with an emphasis on Daidzein, Oxid. Med. Cell. Longev. 2021 (2021), https://doi.org/10.1155/2021/6331630.

[27] R. Samanta, A. Pattnaik, K. Pradhan, B. Mehta, S. Pattanayak, S. Banerjee, Wound healing activity of silibinin in mice, Pharmacogn. Res. 8 (2016) 298–302, https://doi.org/10.4103/0974-8490.188880.

[28] J. Serrano-Román, P. Nicasio-Torres, E. Hernández-Pérez, E. Jiménez-Ferrer, Elimination pharmacokinetics of sphaeralcic acid, tomentin and scopoletin mixture from a standardized fraction of Sphaeralcea angustifolia (Cav.) G. Don orally administered, J. Pharm. Biomed. Anal. 183 (2020), 113143, https://doi.org/10.1016/j.jpba.2020.113143.

[29] J.K. Cho, M.J. Curtis-Long, K.H. Lee, D.W. Kim, H.W. Ryu, H.J. Yuk, K.H. Park, Geranylated flavonoids displaying SARS-CoV papain-like protease inhibition from the fruits of Paulownia tomentosa, Bioorg. Med. Chem. 21 (2013) 3051–3057, https://doi.org/10.1016/j.bmc.2013.03.027.

[30] C. lei Cheng, X. hui Jia, C. mei Xiao, W. zhao Tang, Paulownia C-geranylated flavonoids: their structural variety, biological activity and application prospects,

Phytochemistry Rev. 18 (2019) 549–570, https://doi.org/10.1007/S11101-019-09614-2/TABLES/6.
[31] M. Iranshahi, R. Rezaee, H. Parhiz, A. Roohbakhsh, F. Soltani, Protective effects of flavonoids against microbes and toxins: the cases of hesperidin and hesperetin, Life Sci. 137 (2015) 125–132, https://doi.org/10.1016/j.lfs.2015.07.014.
[32] S. Li, H. Wang, L. Guo, H. Zhao, C.T. Ho, Chemistry and bioactivity of nobiletin and its metabolites, J. Funct.Foods 6 (2014) 2–10, https://doi.org/10.1016/j.jff.2013.12.011.
[33] D. Fang, Z. Xiong, J. Xu, J. Yin, R. Luo, Chemopreventive mechanisms of galangin against hepatocellular carcinoma: a review, Biomed. Pharmacother. 109 (2019) 2054–2061, https://doi.org/10.1016/J.BIOPHA.2018.09.154.
[34] S. Yu, H. Yan, L. Zhang, M. Shan, P. Chen, A. Ding, S.F.Y. Li, A review on the phytochemistry, pharmacology, and pharmacokinetics of amentoflavone, a naturally-occurring biflavonoid, Molecules 22 (2017) 299, https://doi.org/10.3390/MOLECULES22020299, 22 (2017) 299.
[35] X. Feng, X. Zhang, Y. Chen, L. Li, Q. Sun, L. Zhang, Identification of bilobetin metabolites, in vivo and in vitro, based on an efficient ultra-high-performance liquid chromatography coupled with quadrupole time-of-flight mass spectrometry strategy, J. Separ. Sci. 43 (2020) 3408–3420, https://doi.org/10.1002/JSSC.202000313.
[36] V.R.P.S. Kiran, R.P.B. P, Flavonoid: a review on Naringenin, J. Pharmacogn. Phytochem. 6 (2017) 2778–2783. https://www.phytojournal.com/archives/2017.v6.i5.2042/flavonoid-a-review-on-naringenin. (Accessed 4 February 2022).
[37] H. Liu, Y. Dong, Y. Gao, Z. Du, Y. Wang, P. Cheng, A. Chen, H. Huang, The fascinating effects of Baicalein on cancer: a review, Int. J. Mol. Sci. 17 (2016) 1681, https://doi.org/10.3390/IJMS17101681, 17 (2016) 1681.
[38] X. Song, L. Tan, M. Wang, C. Ren, C. Guo, B. Yang, Y. Ren, Z. Cao, Y. Li, J. Pei, Myricetin, A review of the most recent research, Biomed. Pharmacother. 134 (2021), 111017, https://doi.org/10.1016/J.BIOPHA.2020.111017.
[39] A. Hosseini, B.M. Razavi, M. Banach, H. Hosseinzadeh, Quercetin and metabolic syndrome: a review, Phyther. Res. 35 (2021) 5352–5364, https://doi.org/10.1002/PTR.7144.
[40] M. Imran, A. Rauf, Z.A. Shah, F. Saeed, A. Imran, M.U. Arshad, B. Ahmad, S. Bawazeer, M. Atif, D.G. Peters, M.S. Mubarak, Chemo-preventive and therapeutic effect of the dietary flavonoid kaempferol: a comprehensive review, Phyther. Res. 33 (2019) 263–275, https://doi.org/10.1002/PTR.6227.
[41] Z. Jin, X. Du, Y. Xu, Y. Deng, M. Liu, Y. Zhao, B. Zhang, X. Li, L. Zhang, C. Peng, Y. Duan, J. Yu, L. Wang, K. Yang, F. Liu, R. Jiang, X. Yang, T. You, X. Liu, X. Yang, F. Bai, H. Liu, X. Liu, L.W. Guddat, W. Xu, G. Xiao, C. Qin, Z. Shi, H. Jiang, Z. Rao, H. Yang, Structure of Mpro from COVID-19 virus and discovery of its inhibitors, bioRxiv (2020) 2020, https://doi.org/10.1101/2020.02.26.964882, 02.26.964882.
[42] R. Yan, Y. Zhang, Y. Li, L. Xia, Y. Guo, Q. Zhou, Structural basis for the recognition of SARS-CoV-2 by full-length human ACE2, Science 367 (2020) 1444–1448, https://doi.org/10.1126/science.abb2762.
[43] G.M. Morris, R. Huey, W. Lindstrom, M.F. Sanner, R.K. Belew, D.S. Goodsell, A. J. Olson, AutoDock4 and AutoDockTools4: automated docking with selective receptor flexibility, J. Comput. Chem. 30 (2009) 2785–2791, https://doi.org/10.1002/jcc.21256.
[44] M. Tahir ul Qamar, S.M. Alqahtani, M.A. Alamri, L.L. Chen, Structural basis of SARS-CoV-2 3CLpro and anti-COVID-19 drug discovery from medicinal plants, J. Pharm. Anal. 10 (2020) 313–319, https://doi.org/10.1016/j.jpha.2020.03.009.
[45] K. Onodera, K. Satou, H. Hirota, Evaluations of molecular docking programs for virtual screening, J. Chem. Inf. Model. 47 (2007) 1609–1618, https://doi.org/10.1021/ci7000378.
[46] L.L.G. Ferreira, A.D. Andricopulo, ADMET modeling approaches in drug discovery, Drug Discov. Today 24 (2019) 1157–1165, https://doi.org/10.1016/j.drudis.2019.03.015.
[47] J.C. Phillips, R. Braun, W. Wang, J. Gumbart, E. Tajkhorshid, E. Villa, C. Chipot, R. D. Skeel, L. Kalé, K. Schulten, Scalable molecular dynamics with NAMD, J. Comput. Chem. 26 (2005) 1781–1802, https://doi.org/10.1002/JCC.20289.
[48] S. Jo, T. Kim, V.G. Iyer, W. Im, CHARMM-GUI: a web-based graphical user interface for CHARMM, J. Comput. Chem. 29 (2008) 1859–1865, https://doi.org/10.1002/JCC.20945.
[49] P. Mark, L. Nilsson, Structure and dynamics of the TIP3P, SPC, and SPC/E water models at 298 K, J. Phys. Chem. 105 (2001) 9954–9960, https://doi.org/10.1021/JP003020W.
[50] W. Im, S. Seefeld, B. Roux, A grand canonical Monte Carlo–brownian dynamics algorithm for simulating ion channels, Biophys. J. 79 (2000) 788–801, https://doi.org/10.1016/S0006-3495(00)76336-3.
[51] W. Humphrey, A. Dalke, K. Schulten, VMD: visual molecular dynamics, J. Mol. Graph. 14 (1996) 33–38, https://doi.org/10.1016/0263-7855(96)00018-5.
[52] P.A. Kollman, I. Massova, C. Reyes, B. Kuhn, S. Huo, L. Chong, M. Lee, T. Lee, Y. Duan, W. Wang, O. Donini, P. Cieplak, J. Srinivasan, D.A. Case, T.E. Cheatham, Calculating structures and free energies of complex molecules: combining molecular Mechanics and continuum models, Acc. Chem. Res. 33 (2000) 889–897, https://doi.org/10.1021/AR000033J.
[53] B.R. Miller, T.D. McGee, J.M. Swails, N. Homeyer, H. Gohlke, A.E. Roitberg, MMPBSA.py: an efficient program for end-state free energy calculations, J. Chem. Theor. Comput. 8 (2012) 3314–3321, https://doi.org/10.1021/CT300418H.
[54] A. Onufriev, D. Bashford, D.A. Case, Exploring protein native states and large-scale conformational changes with a modified generalized born model, Proteins 55 (2004) 383–394, https://doi.org/10.1002/PROT.20033.
[55] J. Weiser, P.S. Shenkin, W.C. Still, Approximate atomic surfaces from linear combinations of pairwise overlaps (LCPO), J. Comput. Chem. 20 (1999) 217–230. https://onlinelibrary.wiley.com/doi/abs/10.1002/(SICI)1096-987X(19990130)20:2%3C217::AID-JCC4%3E3.0.CO;2-A. (Accessed 29 May 2022).
[56] S. Genheden, U.L.F. Ryde, How to obtain statistically converged MM/GBSA results, J. Comput. Chem. 31 (2010) 837–846, https://doi.org/10.1002/JCC.21366.
[57] I. Massova, P.A. Kollman, Combined molecular mechanical and continuum solvent approach (MM-PBSA/GBSA) to predict ligand binding, Perspect. Drug Discov. Des. 18 (2000) 113–135, https://doi.org/10.1023/A:1008763014207.
[58] F. Adasme-Carreño, C. Muñoz-Gutierrez, J. Caballero, J.H. Alzate-Morales, Performance of the MM/GBSA scoring using a binding site hydrogen bond network-based frame selection: the protein kinase case, Phys. Chem. Chem. Phys. 16 (2014) 14047–14058, https://doi.org/10.1039/C4CP01378F.
[59] H.S.H. Mohammed Ali, H.N. Altayb, A.A.M. Bayoumi, A. El Omri, A. Firoz, K. Chaieb, In Silico Screening of the Effectiveness of Natural Compounds from Algae as SARS-CoV-2 Inhibitors: Molecular Docking, ADMT Profile and Molecular Dynamic Studies, 2022, https://doi.org/10.1080/07391102.2022.2046640.
[60] J.H. Zothantluanga, M. Abdalla, M. Rudrapal, Q. Tian, D. Chetia, J. Li, Computational Investigations for Identification of Bioactive Molecules from Baccaurea Ramiflora and Bergenia Ciliata as Inhibitors of SARS-CoV-2 Mpro, 2022, https://doi.org/10.1080/10406638.2022.2046613.
[61] V. Kumar, S. Kar, P. De, K. Roy, J. Leszczynski, Identification of Potential Antivirals against 3CLpro Enzyme for the Treatment of SARS-CoV-2: A Multi-step Virtual Screening Study, 2022, pp. 357–386, https://doi.org/10.1080/1062936X.2022.2055140.
[62] B. Jawad, P. Adhikari, R. Podgornik, W.Y. Ching, Key interacting residues between RBD of SARS-CoV-2 and ACE2 receptor: combination of molecular dynamics simulation and density functional calculation, J. Chem. Inf. Model. 61 (2021) 4425–4441, https://doi.org/10.1021/ACS.JCIM.1C00560/SUPPL_FILE/CI1C00560_SI_002.XLSX.
[63] H. Hadni, M. Elhallaoui, 2D and 3D-QSAR, molecular docking and ADMET properties in silico studies of azaaurones as antimalarial agents, New J. Chem. (2020), https://doi.org/10.1039/c9nj05767f.
[64] H. Hadni, M. Elhallaoui, 3D-QSAR, docking and ADMET properties of aurone analogues as antimalarial agents, Heliyon 6 (2020), e03580, https://doi.org/10.1016/j.heliyon.2020.e03580.
[65] J. Kirchmair, P. Markt, S. Distinto, G. Wolber, T. Langer, Evaluation of the performance of 3D virtual screening protocols: RMSD comparisons, enrichment assessments, and decoy selection - what can we learn from earlier mistakes? J. Comput. Aided Mol. Des. 22 (2008) 213–228, https://doi.org/10.1007/s10822-007-9163-6.
[66] A. Daina, O. Michielin, V. Zoete, SwissADME: a free web tool to evaluate pharmacokinetics, drug-likeness and medicinal chemistry friendliness of small molecules, Sci. Rep. 7 (2017), https://doi.org/10.1038/srep42717.
[67] D.E.V. Pires, T.L. Blundell, D.B. Ascher, pkCSM: predicting small-molecule pharmacokinetic and toxicity properties using graph-based signatures, J. Med. Chem. 58 (2015) 4066–4072, https://doi.org/10.1021/acs.jmedchem.5b00104.
[68] M. Babayeva, Z. Loewy, Repurposing drugs for COVID-19: pharmacokinetics and pharmacogenomics of chloroquine and hydroxychloroquine, Pharmgenomics. Pers. Med. 13 (2020) 531–542, https://doi.org/10.2147/PGPM.S275964.
[69] S. Agarwal, S.K. Agarwal, Lopinavir-ritonavir in SARS-CoV-2 infection and drug-drug interactions with cardioactive medications, Cardiovasc. Drugs Ther. (2020) 1–14, https://doi.org/10.1007/s10557-020-07070-1.
[70] S. Beura, P. Chetti, In-silico strategies for probing chloroquine based inhibitors against SARS-CoV-2, J. Biomol. Struct. Dyn. 39 (2021) 3747–3759, https://doi.org/10.1080/07391102.2020.1772111.